

Significant Inverse Magnetocaloric Effect induced by Quantum Criticality

Tao Liu,^{1,2,*} Xin-Yang Liu,^{2,*} Yuan Gao,² Hai Jin,³ Jun He,¹ Xian-Lei Sheng,² Wentao Jin,²
Ziyu Chen,^{2,†} and Wei Li^{2,4,5,‡}

¹*School of Science, Hunan University of Technology, Zhuzhou 412007, China*

²*School of Physics, Beihang University, Beijing 100191, China*

³*Department of Astronomy, Tsinghua Center for Astrophysics, Tsinghua University, Beijing 100084, China*

⁴*International Research Institute of Multidisciplinary Science, Beihang University, Beijing 100191, China*

⁵*Institute of Theoretical Physics, Chinese Academy of Sciences, Beijing 100190, China*

(Dated: March 2, 2022)

The criticality-enhanced magnetocaloric effect (MCE) near a field-induced quantum critical point (QCP) in the spin systems constitutes a very promising and highly tunable alternative to conventional adiabatic demagnetization refrigeration. Strong fluctuations in the low- T quantum critical regime can give rise to a large thermal entropy change and thus significant cooling effect when approaching the QCP. In this work, through efficient and accurate many-body calculations, we show there exists a significant inverse MCE (iMCE) in the spin-1 quantum chain materials $(\text{CH}_3)_4\text{NNi}(\text{NO}_2)_3$ (TMNIN) and $\text{NiCl}_2\text{-4SC}(\text{NH}_2)_2$ (DTN), where DTN has substantial low- T refrigeration capacity while requiring only moderate magnetic fields. The iMCE characteristics, including the adiabatic temperature change ΔT_{ad} , isothermal entropy change ΔS , differential Grüneisen parameter, and the entropy change rate, are obtained with quantum many-body calculations at finite temperature. The cooling performance, i.e., the efficiency factor and hold time, of the two compounds is also discussed. Based on the many-body calculations on realistic models for the spin-chain materials, we conclude that the compound DTN constitutes a very promising and highly efficient quantum magnetic coolant with pronounced iMCE properties. We advocate that such quantum magnets can be used in cryofree refrigeration for space applications and quantum computing environments.

I. INTRODUCTION

The magnetocaloric effect (MCE) represents a significant adiabatic temperature change of a magnet as a response to the varying external magnetic fields [1–4]. Historically, the first sub-Kelvin regime cooling was realized through adiabatic demagnetization refrigeration (ADR) [5]. Recently, low- T magnetic refrigeration gets refreshed research interest due to its important applications in space technology [6, 7] and the cryofree sub-Kelvin environment for quantum computers [8]. It is of great research interest to pursue novel MCE refrigerants that provide higher cooling powers and can reach lower temperatures. Among others, the quantum spin-chain materials with enhanced MCE characterized by the universally diverging Grüneisen ratio near the quantum critical point (QCP) [9–15], has been proposed as a very promising quantum critical coolant for magnetic refrigeration [16, 17] and an excellent alternative to the conventional ADR.

In most magnetic materials, the spin degrees of freedom in the system eventually “solidify” into a long-range order as cooled down to sufficiently low temperatures. In such magnetically ordered phase, the spin states are practically non-tunable by external fields (due to the existence of giant Weiss molecular fields) and the corresponding MCE, temperature or entropy change as a response to fields, are usually negligible. Paramagnetic salts, like $\text{CrK}(\text{SO}_4)_2 \cdot 12\text{H}_2\text{O}$ (Chromic Potassium Alum, CPA) and $\text{Fe}(\text{SO}_4)_2\text{NH}_4 \cdot 2\text{H}_2\text{O}$ (Ferric Ammonium Alum, FAA), etc, host nearly non-interacting spins and

do not order at very low temperatures, are widely used in ADR as spin “gas” refrigerant [7]. It is commonly believed that the spin interactions are “harmful” for good ADR coolants, as they usually lead to magnetic ordering as T lowers and spoil the MCE properties.

Nevertheless, there is exotic exception to this classic fate of interacting quantum spins. In low dimensional quantum magnets [18], the quantum fluctuations can be strong enough to prevent the spins from classical ordering even at $T = 0$. One prominent case is the field-induced QCP in the correlated quantum magnetic materials. The enhanced quantum fluctuations near the QCP can significantly influence the thermodynamics in the quantum critical regime at low temperature [19]. When approaching the QCP, the spin system would experience a significant isothermal entropy change, which can be translated into a considerable temperature decrease under the adiabatic condition. Such quantum criticality-enhanced MCE is reflected in a diverging Grüneisen parameter [adiabatic temperature change rate, cf. Eq.(2) below], $\Gamma_B \sim T^{-1/z\nu}$ under external field B , with z and ν the dynamical and critical exponents related to the universality class of the QCP [11, 12]. Notably, such intriguing quantum critical phenomena in low-temperature thermodynamics also provides a sensitive probe of QCP in experiments [20].

The low-temperature thermodynamic properties of a typical 1D quantum magnetic system — the spin-1/2 Heisenberg chain (HAFC) — have been intensively explored, where a pronounced MCE was predicted [9, 10] and also observed in the compound $[\text{Cu}(\mu\text{-C}_2\text{O}_4)(4\text{-aminopyridine})_2(\text{H}_2\text{O})]_n$ (CuP). The lowest achievable temperature with the spin-chain coolants has no principal limitation (as long as the inter-chain interactions are negligible), and the high efficiency factor as well as long hold time makes the spin-1/2 HAFC materials

* These authors contributed equally to this work.

† chenzy@buaa.edu.cn

‡ w.li@buaa.edu.cn

very promising quantum critical refrigerants [16, 17].

Nevertheless, there is still plenty of room for further improving the performance of quantum magnetic refrigerants. As reported in Ref. [16], for the spin-1/2 HAFC compound CuP, one has to start from a rather high magnetic field, e.g., 7 T, significantly above the critical field $B_c \simeq 4.09$ T. In CuP, there indeed exists significant MCE in the range $B > B_c$, while in the smaller-field side, i.e., $B \in [0, B_c]$, rather weak (inverse) MCE was observed. Therefore, the generated strong magnetic fields (of 7 T) have actually not been fully exploited in the case of spin-1/2 compound CuP. On the other hand, popular paramagnetic refrigerants are typically with high spin $S \geq 1$, as larger entropy changes are generally expected for higher spin systems. For example, CPA and FAA are with $S = 3/2$ and $5/2$, respectively, and the Gadolinium Gallium Garnet (GGG) is even with $S = 7/2$. However, there is only a few studies on quantum spin models [13] and materials [15] with spin higher than $S = 1/2$.

In this work, we systematically investigate the iMCE properties of the $S = 1$ quantum chain models and materials with many-body simulations. Special emphases are put on two typical spin-1 HAFC materials, i.e., $(\text{CH}_3)_4\text{NNi}(\text{NO}_2)_3$ (TMNIN) and $\text{NiCl}_2\text{-}4\text{SC}(\text{NH}_2)_2$ (DTN), whose magneto-thermodynamic properties can be accurately simulated by the thermal-state linearized tensor renormalization group (LTRG) approaches [21, 22]. In particular, we find the compound DTN has iMCE refrigeration capacity comparable to the MCE of spin-1/2 HAFC material CuP, while requiring only a moderate external magnetic field of $B_c \simeq 3$ T in the cooling process, much smaller than the latter requires. Due to the pronounced cooling effects and excellent thermal transport properties [23] in DTN, we propose DTN constitutes a very promising iMCE refrigerant with only a moderate magnetic field and competitive performance, very suitable for practical refrigeration applications.

The rest parts of the article is arranged as follows. We present the spin-1 chain models, their thermal many-body simulations, and the related spin-1 materials in Sec. II. Our main results on iMCE of the spin-1 chains are shown in Sec. III, and Section IV is devoted to the conclusion and outlook.

II. SPIN-1 HEISENBERG-CHAIN MODEL AND MATERIALS

A. Heisenberg antiferromagnetic chain and tensor renormalization group

The $S = 1$ HAFC systems with single-ion anisotropy can be described by the Hamiltonian

$$\mathcal{H} = \sum_i \left[J \vec{S}_i \cdot \vec{S}_{i+1} + D(S_i^z)^2 + g\mu_B B S_i^z \right], \quad (1)$$

where \vec{S}_i is the spin-1 operator on site i (with S_i^z its z component), J is the nearest-neighbor Heisenberg interaction, and D the single-ion anisotropy parameter. In the Zeeman term, B

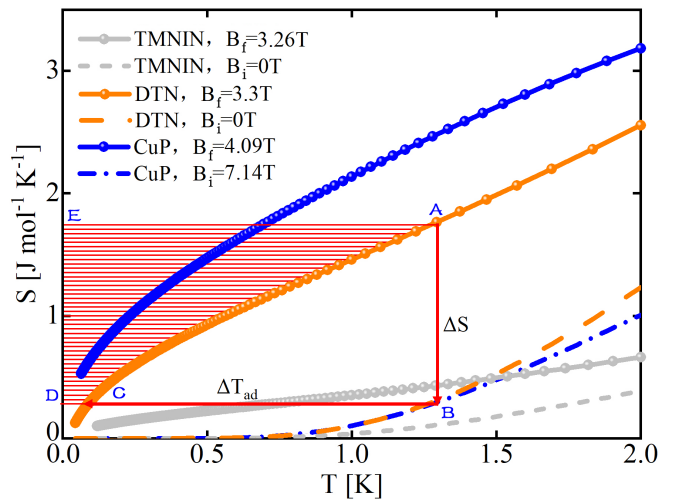


FIG. 1. Simulated thermal entropy $S(T)$ curves of three spin-chain materials, under different initial fields B_i and final fields $B_f = B_c$. Entropy change ΔS (indicated by the vertical red arrow) and adiabatic temperature change ΔT_{ad} (horizontal red arrow) are shown explicitly for the compound DTN. A-B-C-A constitutes a single-shot refrigeration process, and the dashed regime ACDE represents the heat absorbed from the load in the iso-field CA process.

is the external magnetic field, g is the electronic Landé factor, and μ_B the Bohr magneton.

In a rather wide parameter regime [24, 25], the spin-1 chain model Eq.(1) has a non-magnetic ground state with finite spin gap, which can be closed by applying a magnetic field B through the field-induced quantum phase transition. In particular, for the case $D = 0$, the model in Eq.(1) reduces to the isotropic spin-1 HAFC model with the renowned Haldane gap $\Delta \approx 0.41J$ [26–28], where the first excited state is in a spin triplet $S = 1$ sector. The introduction of D in the spin chain can alter the size of Haldane gap, and drive the system into a trivial large- D phase through a topological quantum phase transition at $D/J = 0.93$ [29]. For $D > D_c$, the gap reopens and scales proportional with D in the large- D limit. Besides, other off-diagonal single-ion anisotropies are found to be small in the two spin-1 chain compounds — TMNIN and DTN — considered in the present work, and we thus set them to zero in the rest of our discussion.

To simulate the finite-temperature properties and characterize the iMCE properties of the spin-1 chain materials, we employ the infinite-size LTRG method [21] in the bilayer form [22] for high-precision thermal many-body calculations down to low temperature $T/J = 0.01$. In the process of imaginary-time evolution (cooling), we retain up to $\chi = 400$ bond states (with truncation error $\epsilon \lesssim 10^{-5}$) in the matrix-product thermal density operator, which always guarantees accurate and converged thermodynamic results.

Compound	Abbr.	$J/k_B(\text{K})$	$D/k_B(\text{K})$	$\Delta/k_B(\text{K})$	g	$B_c(\text{T})$	Reference
$(\text{CH}_3)_4\text{NNi}(\text{NO}_2)_3$	TMNIN	11.7 – 12	-	4.1 – 4.5	2.22 – 2.25	3	[30–33]
$\text{NiCl}_2\text{-4SC}(\text{NH}_2)_2$	DTN	2.2	8.9	3.2	2.26	2.13 ^a	[23, 34–38]
$\text{Ni}(\text{C}_2\text{H}_8\text{N}_2)_2\text{NO}_2\text{BF}_4$	NENB	44.8 – 47.7	7.5	17.4	2.14	9 – 13	[15, 39]
$\text{Ni}(\text{C}_2\text{H}_8\text{N}_2)_2\text{NO}_2\text{ClO}_4$	NENP	46.2 – 48	10 – 16	13 – 7	2.1 – 2.2	9.8 – 13.4	[40, 41]
$\text{Ni}(\text{C}_3\text{H}_{10}\text{N}_2)_2\text{NO}_2\text{ClO}_4$	NINO	50 – 52	11.5 – 16	10 – 15	2.2	8.9 – 11.2	[42, 43]
$\text{Ni}(\text{C}_3\text{H}_{10}\text{N}_2)_2\text{N}_3\text{ClO}_4$	NINAZ	100 – 145	-	30 – 44	-	-	[31, 44]
Y_2BaNiO_5	-	250 – 280	50 – 56	60.5 – 110	2.16	-	[45, 46]

^a The experimentally measured critical field is 2.2 T in DTN, smaller than the theoretical 1D results of about 3.3 T, due to the influence of inter-chain interactions.

TABLE I. Some common spin-1 chain compounds and their microscopic Hamiltonian parameters, including the intra-chain exchange J , uniaxial single ion anisotropy D , the spin excitation gap Δ , the Landé factor g , and the (lower) critical field B_c . The magnets are listed in ascending order in strength of the Heisenberg coupling J .

B. iMCE property and performance characteristics

Driven by external magnetic fields, the spin-1 chains in the quantum critical regime show significantly enhanced MCE. To quantitatively characterize the MCE property, we calculate the magnetic Grüneisen parameter

$$\Gamma_B = \frac{1}{T} \left(\frac{\partial T}{\partial B} \right)_S = -\frac{1}{C_B} \left(\frac{\partial M}{\partial T} \right)_B, \quad (2)$$

with $C_B = T(\partial S/\partial T)_B$ the magnetic specific heat (under an external field B). The Grüneisen parameter Γ_B measures the temperature change rate as a response to the small variation of the external field under an adiabatic condition. In the numerator of Eq. (2) is a related differential quantity

$$\Theta_T = \left(\frac{\partial S}{\partial B} \right)_T = \left(\frac{\partial M}{\partial T} \right)_B,$$

which measures the isothermal entropy change rate.

Correspondingly, when integrated over a given range of fields, e.g., $B \in [B_i, B_f]$ with B_i and B_f the initial and final (critical) fields in the iMCE process, respectively. The isothermal entropy change is

$$\Delta S(T) = \int_{B_i}^{B_f} \left(\frac{\partial S}{\partial B} \right)_T dB = \int_{B_i}^{B_f} \left(\frac{\partial M}{\partial T} \right)_B dB,$$

and the adiabatic temperature change is

$$\Delta T_{\text{ad}} = \int_{B_i}^{B_f} \Gamma_B T dB = - \int_{B_i}^{B_f} \frac{T}{C_B} \left(\frac{\partial M}{\partial T} \right)_B dB.$$

Besides the above MCE property characteristics, in practical applications the refrigeration efficiency factor η and hold time are important quantities measuring their cooling performance. The efficiency factor is defined as the ratio $\eta = \Delta Q_c/\Delta Q_m$, where $\Delta Q_c = \int_{T_f}^{T_i} T (\partial S/\partial T)_{B_f} dT$ refers to the heat absorption from load (indicated by the red shadow area ACDE in Fig. 1), and $\Delta Q_m = T_i \cdot [S(B_f, T_i) - S(B_i, T_i)]$ is the heat exchange between the material and the heat reservoir at the high temperature T_i . In

multistage single-shot or continuous ADRs, the whole system must be optimized according to the pre-cooling requirements and total weight, in which the efficiency factor is to be crucial [7]. Besides, the hold time — reflecting the temperature-time curve of the refrigerant in contact with constant heat load — is another important parameter for an efficient refrigeration. The refrigerant temperature is defined as $T_S(t) = T_S(0) + \dot{Q}/C_m$, and particularly we require the refrigerant temperature does not increase too rapidly (thus a long hold time), under a constant heat load \dot{Q} .

C. Spin-1 Chain Quantum Magnets

Distinct from the spin-1/2 chains, the spin-1 HAFC system has a gapped ground states [27, 28] with symmetry-protected topological (STP) order [47]. There has been continuous research interest in the investigation of the spin-1 chain materials, with some prominent examples listed in Tab. I. In these compounds, there exists single-ion anisotropy term D [cf. Eq. (1)] besides the Heisenberg interaction J . In this work, we are particularly interested in the compounds TMNIN [30–33] and DTN [23, 34–38], due to their very moderate critical field strength $B_c \leq 3$ T (cf. Tab. I) that is very suitable for magnetic refrigeration applications. Besides these two members, there are other spin-1 chain materials in the family, including NENB [15, 39], NENP [40, 41], and NINO [42, 43] (cf. Tab. I), which are very common frustration-free spin-1 materials that can be described by the Hamiltonian Eq. (1).

Despite a little dispute about the specific value of J and Landé factor g , consensus has been reached that the compound TMNIN can be well described by a spin-1 HAFC with negligible single-ion anisotropy [30, 33], through fitting the magnetic susceptibility [30], specific heat [32], and magnetization curve [31]. Below, to explore the MCE properties of materials with the corresponding theoretical model, we take the parameter set $J = 12$ K and $g = 2.25$ from Ref. [30] for TMNIN, and choose the set of parameters $J = 2.2$ K, $D = 8.9$ K, and $g = 2.26$ for DTN [35]. Before discussing the iMCE properties and performances of the spin-1 chain refrigerants, we note that TMNIN can be regarded as an excellent

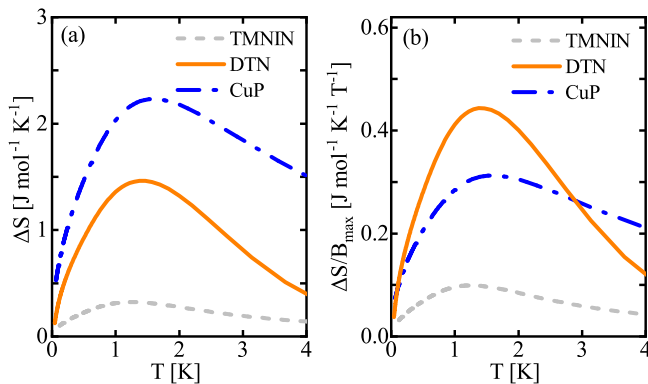


Fig. 2. (a) Simulated molar magnetic entropy change ΔS as a function of temperature T , for three compounds, TMNIN (gray dashed line), DTN (orange line), and CuP (blue dash-dot line). (b) compares the entropy change per Tesla, $\Delta S/B_{\text{max}}$, for three compounds.

spin-1 HAFM material that corresponds to a gapped ground state, while the DTN has $D/J \simeq 4$ and well resides in the trivial large- D phase. TMNIN opens up the spin excitation gap due to the emergence of SPT order, in sharp distinction to gapless spin-1/2 materials like CuP. Therefore, it is interesting to compare iMCE of these two materials as *topological* Haldane vs. trivial large- D magnetic refrigerants.

III. INVERSE MCE IN THE SPIN-1 CHAIN MATERIALS

Below we provide our main results of magnetothermodynamics of two spin-1 chain magnets, the Haldane chain TMNIN and large- D chain DTN, and compare them to the spin-1/2 HAFM compound CuP (with parameters $J = 3.2$ K and $g = 2.33$ [48]). We show the MCE characteristics, including the adiabatic temperature change ΔT_{ad} , isothermal entropy change ΔS , Güneisen parameter Γ_B , and differential characterization Θ_T , etc. The practical cooling performance like the efficiency factor η and hold time are also discussed and compared in this section.

A. Entropy curves and isothermal entropy change ΔS

Magnetic fields can tune the spin states of the system and induce significant entropy change that can then be transferred into cooling effects. In Fig. 1, we show the entropy curves at two magnetic fields — the initial field B_i and the final field B_f . As we are considering the iMCE process, they are set as $B_i = 0, B_f = 3.26$ T (TMNIN) and $B_i = 0, B_f = 3.3$ T (DTN) for the two spin-1 compounds. It should be noted that in the iMCE process the largest required field (here B_f) is right the critical field value (B_c). This is in sharp contrast to the MCE process of spin-1/2 material CuP, where $B_f = 4.09$ T (also at the QCP) and the largest field in the cooling procedure is instead $B_i = 7.14$ T, much greater than

that required in the compounds TMNIN and DTN. Such significant reduction of the maximal magnetic fields is important for the implementation of the quantum magnetic refrigeration in, say, the space applications.

From the thermal entropy curves in Fig. 1, we find the Haldane magnet TMNIN has a rather small isothermal entropy change ΔS , clearly less than $1 \text{ J mol}^{-1} \text{ K}^{-1}$ regardless of the working temperature (cf. Fig. 2). However, the large- D magnet DTN is found to conduct quite prominent entropy change, as seen in Figs. 1 and 2, comparable to that of the spin-1/2 compound CuP. As DTN only requires a maximal field ($B_{\text{max}} = B_f = 3.3$ T), half of that for CuP, we find DTN has the highest “efficiency”, i.e., entropy change per Tesla, over the other two compounds as shown in Fig. 2(b).

B. Isentropes and adiabatic temperature change ΔT_{ad}

In the iMCE cooling procedure, the compounds are firstly magnetized along the isothermal line AB (red arrowed line in Fig. 1). A larger ΔS means the greater cooling capacity, which, in the adiabatic process (indicated by the horizontal line BC) is translated into a large temperature change ΔT_{ad} . When the magnet reaches its lowest temperature T_f at the point C, we contact the refrigerant with the heat load and it starts to absorb heat from there. The temperature of the magnetic refrigerant gradually rises up along the iso-field line CA with a fixed field B_f .

On this basis, it becomes very meaningful to compute the isentropes of the three compounds and determine the adiabatic temperature change ΔT_{ad} from there. In Fig. 3(a,b), we show isentropes of TMNIN and DTN, where the criticality-enhanced iMCE can be clearly observed. When the magnetic field increases from zero ($B_i = 0$) to critical field ($B_f \geq B_c \simeq 3$ T for both spin-1 compounds), we find the temperature decreases monotonically, e.g., from about 2 K to about 1 K (for TMNIN) and 500 mK (DTN). The ΔT_{ad} results are collected and shown in Fig. 4, which are found significant in the course of increasing fields for both TMNIN and DTN, in a wide range of initial temperatures T_i shown up to 2.5 K.

In the isentropes of DTN (and also TMNIN) in Fig. 3, we can recognize two dips in low- T isentropic lines, which correspond to the two field-driven QCP. The lower-field one (at about 3.3 T for DTN) with strong iMCE occurring due to the closure of spin gap, while the one at higher field (about 11.7 T for DTN) is the saturation transition where the spins become polarized. Different from the spin-1 chains, the results of spin-1/2 CuP in Fig. 3(c) show only one saturation QCP at a field of about $B_c \simeq 4$ T. If we increase the fields from zero to B_c , the iMCE in CuP is apparently weak; while the MCE in CuP is significant when decreasing from a large B_i higher than 7 T [cf. Figs. 3(c) and 4(a)]. Therefore, to make a fair comparison, we compute the temperature change ΔT_{ad} per Tesla, i.e., $\Delta T_{\text{ad}}/B_{\text{max}}$, in Fig. 4(b). From the same (high) initial temperatures $T_i \lesssim 2.5$ K, we find that the DTN actually has the largest ratio, and TMNIN is also more efficient than CuP.

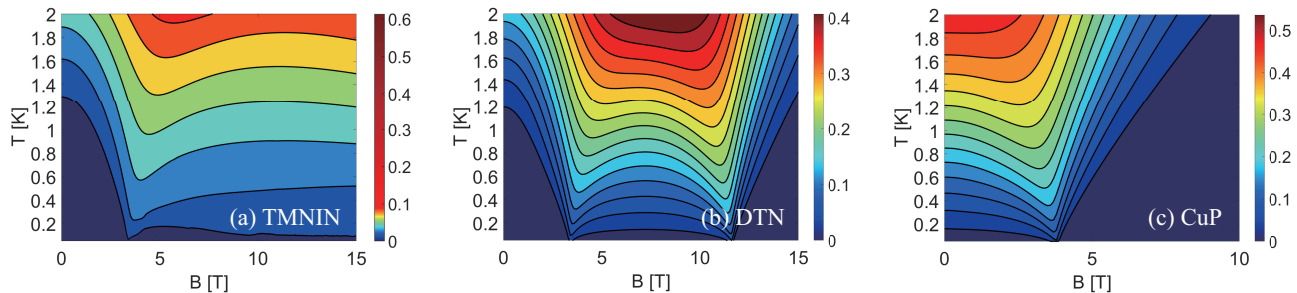


Fig. 3. Simulated isentropic contour plots of three spin-chain compounds, including the spin-1 materials (a) TMNIN and (b) DTN, and (c) the spin-1/2 chain CuP. There are two QCPs at lower (B_c) and upper (B_s) critical fields in panels (a) and (b), where $B_c = 3.26$ T (and $B_s \simeq 32$ T not shown) [49] for TMNIN and $B_c = 3.3$ T, $B_s = 11.7$ T for DTN. Between B_c and B_s there exists a continuous Tomonaga-Luttinger liquid (TLL) regime with relatively flat isentropic lines at low temperature.

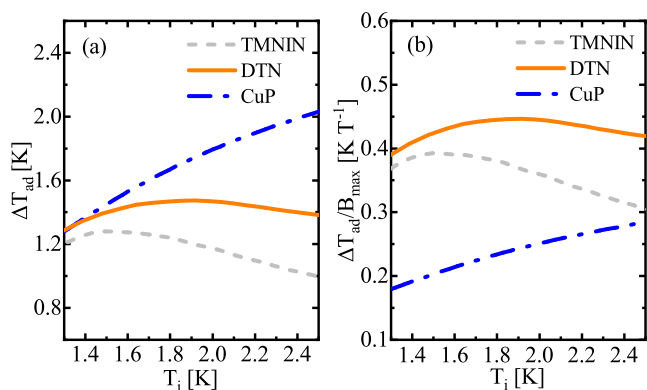


Fig. 4. (a) The adiabatic temperature change ΔT_{ad} and (b) temperature change per Tesla, $\Delta T_{\text{ad}}/B_{\text{max}}$ of three spin-chain compounds considered in this work.

C. Grüneisen parameter Γ_B and differential iMCE Θ_T

Above we have computed the isothermal entropy change ΔS and adiabatic temperature change ΔT_{ad} of two spin-1 materials, and find that the absolute and per-Tesla values are both important for characterizing iMCE properties. Matter of fact, to compare the MCE properties more faithfully, by getting ride of the influences of different field ranges, we exploit the differential characterizations including the Grüneisen parameter Γ_B and differential entropy change Θ_T . With these we are able to compare the MCE properties point by point at each magnetic field.

The Grüneisen ratios Γ_B of three spin-chain materials are compared in Fig. 5. In all three cases, we find pronounced peaks in Γ_B that change its sign abruptly near the QCP [11, 12], revealing the quantum criticality-enhanced MCE. The height of the Γ peak represents the adiabatic temperature change rate under an infinitesimal field change, which increases as T lowers and diverges as $T \rightarrow 0$ [11]. Again, we see that the Γ_B peaks of TMNIN are much weaker than those of DTN and CuP at the same temperature. The positive peaks

and negative dips represent respectively the MCE and iMCE in the materials, which are quite different for the spin-1 DTN and spin-1/2 CuP materials. For DTN, Γ_B is negative (iMCE) in the small-field side and positive (MCE) on the other, with the negative dip much more pronounced as compared to the positive peak, i.e., the iMCE in DTN is much stronger than MCE. On the contrary, CuP exhibits exactly the reversed behaviors, i.e., with a pronounced MCE peak to the right of the critical field while a very weak iMCE peak on the left. This can be understood as the TLL phase appears at different sides of the QCP in the two compounds CuP and DTN.

The results of entropy change rate Θ_T are shown in Fig. 6, which presents the clear positive peaks (iMCE) and negative dip (MCE) around the critical fields at low temperature. Similar as the observations in Γ_B , TMNIN again have only rather weak peaks(dips) in Θ_T , while DTN has a pronounced peak with height in similar magnitude to the dip in CuP curve [Fig. 6(c)], showing strong iMCE. Both Γ_B and Θ_T display characteristic divergent behaviors close to the QCP and change signs as the field crosses the critical point, indicating the pronounced refrigeration effects through adiabatic demagnetization (MCE) and magnetization (iMCE).

D. iMCE performance: Efficiency factor η and hold time

In practical applications, the refrigeration efficiency factor η and the hold time are of significance to maintain a sustainable and high-efficiency refrigeration procedure. The efficiency factor η is the ratio between heat absorbed Q_c from heat load (i.e., the area of the dashed line between the AC and DE lines in Fig. 1) and the released heat Q_m to the heat reservoir, i.e., $\eta = Q_c/Q_m$. For DTN, the area of red shadow in Fig. 1 is $\Delta Q_c = 0.915$ J/mol, similar to that of the spin-1/2 material CuP with $\Delta Q_c = 1.144$ J/mol, while requiring less than half the field. For the Haldane refrigerant TMNIN, we see a small heat absorption $\Delta Q_c = 0.227$ J/mol, again outperformed by the large- D magnet DTN. Besides the heat absorption, we are also interested in the heat release Q_m in the isothermal process (area of the rectangle ABDE), as those

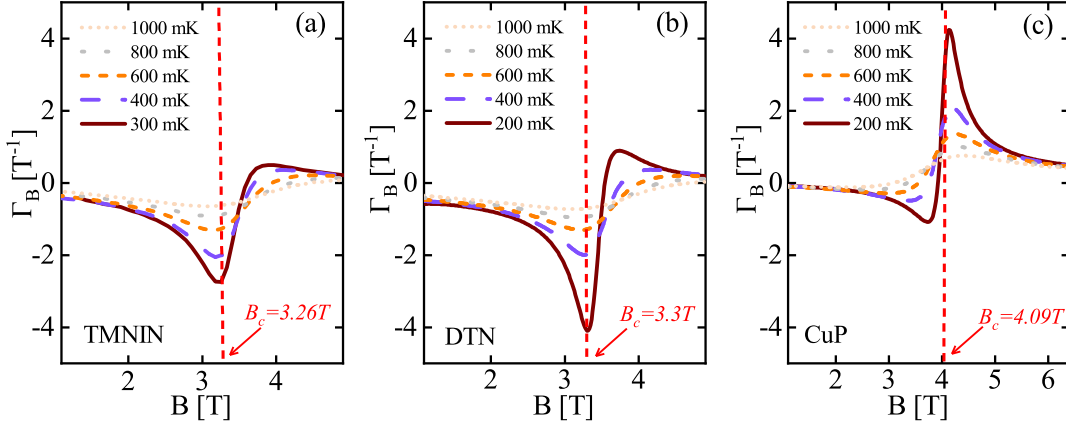


Fig. 5. The simulated Grüneisen parameter Γ_B of three materials, i.e., (a) DTN, (b) CuP, and (c) TMNIN, are shown at various temperatures from 1000 mK down to 200 mK. The red vertical dashed line indicates the critical magnetic fields of the three spin-chain materials.

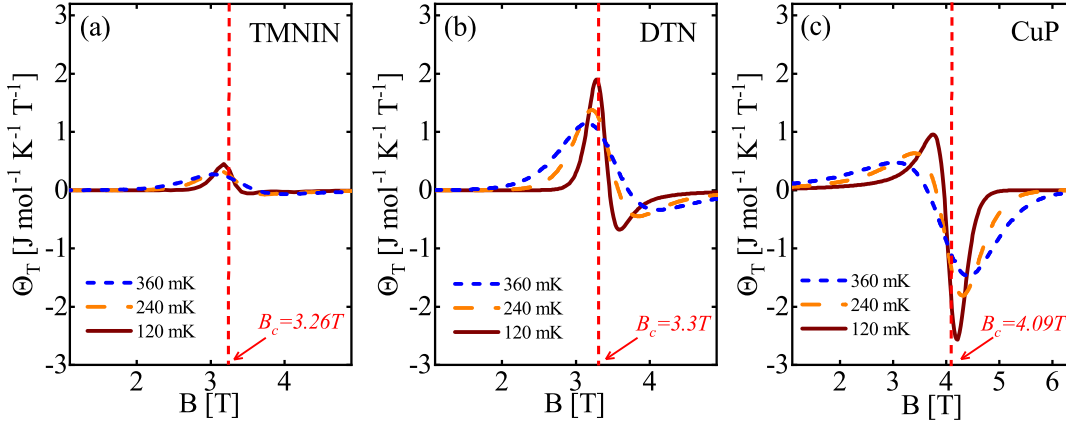


Fig. 6. The simulated entropy change rate Θ_T of three materials, (a) DTN, (b) CuP, and (c) TMNIN, are shown at various temperatures, from 360 mK down to 120 mK.

heat has to be expelled to the outer environment and thus constitutes a load for, e.g., mechanical cooling or higher-stage ADR. For a robust and efficient refrigeration system, we want the refrigerant to absorb Q_c as large as possible while, at the same time, release smaller amount of heat to the environment, i.e., to have a high efficiency factor η [7, 8]. From Fig. 1, we find such a rate of the compound DTN is $\eta = 47.5\%$ when working between $T_i = 1.3$ K and $T_f = 0.09$ K, considerably higher than that of CuP (26% from the same initial temperature T_i as reported in Refs. [16, 17]).

After the adiabatic demagnetization process (BC line in Fig. 1), the refrigerant temperature reaches the lowest value T_f at the magnetic field $B_f = B_c$. After that, the refrigerant contacts with the load and its temperature rises along the iso-field line CA. We want the refrigerant with good performance to absorb heat without warming up too rapidly. The simulated temperature T_S at time t is

$$T_S(t) = T_S(0) + \dot{Q}/C_m,$$

which mainly depends on the magnetic specific heat C_m of

the refrigerant and heat load \dot{Q} . We assume that the heat is transferred at a constant rate $\dot{Q} = 5 \mu\text{W}$ typical for space applications [16], and start from an initial temperature $T_S(0) = 0.01 J/k_B$, where J is the spin coupling constants of the compound. The results, temperature $T_S(t) - T_S(0)$ versus time t , of three compounds are shown in Fig. 7, from which we find the spin-1 DTN has a very similar hold time as that of the spin-1/2 CuP. The hold time of the latter has been shown to be quite competitive as compared to commonly used paramagnetic salts [16]. Overall, we find the spin-1 magnetic refrigerant DTN is of excellent MCE performance in terms of efficiency factor η and hold time.

IV. DISCUSSION AND OUTLOOK

In clear distinct to the paramagnetic ADR, where only isolated ions are involved in the demagnetization cooling process, here in quantum magnetic refrigeration we exploit the correlation and entanglement of the spins and the strong quan-

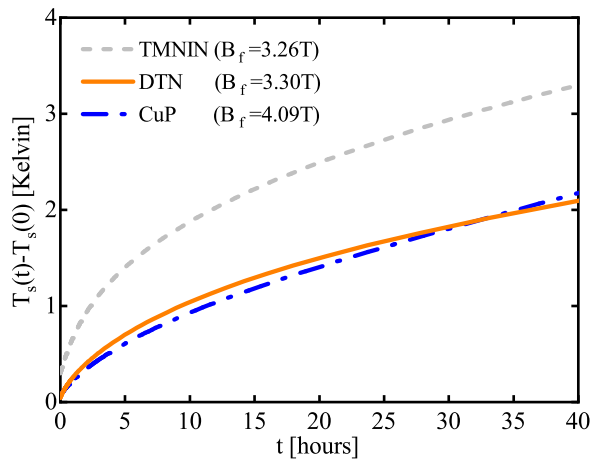


Fig. 7. The sample temperature T_s as a function of time t at a fixed field $B = B_f$, calculated under a constant heat load of $5 \mu W$. We consider 100 g substance of the spin-1/2 CuP (blue dashed line), TMNIN (gray dashed line), and DTN (orange solid line) in the calculations.

tum fluctuations as our resource of cooling capacity, and significant temperature decrease can be gained in both demagnetization (MCE) and magnetization (iMCE) processes. Moreover, different from the conventional (classical) MCE that is most prominent near thermal Curie phase transition at finite temperature, quantum refrigeration is strongly enhanced near the quantum phase transitions at $T = 0$. The strongly fluctuating thermal states near the quantum critical point prevent the constituents, spins, to freeze at low till even zero temperatures, resulting in large entropy change and divergent differential refrigeration characteristics Γ_B and Θ_T , etc, as T goes to zero.

Here we have systematically investigated the iMCE near the field-induced quantum critical point in the spin-1 quantum magnets. As these compounds have a finite spin gap either due to the Haldane topological origin (in TMNIN) or large single-ion effects (DTN), significant iMCE have been observed when the spin gap is closed. In particular, the latter is found to have comparable cooling capacities and even better performances as compared to the criticality-enhanced MCE material CuP, with considerably reduced magnetic fields required.

Moreover, in the compound DTN, the field-induced quantum phase transition can be described as a Bose-Einstein condensation in quantum magnets, and has a high thermal conductivity even at very low temperature [23]. As the typical paramagnetic salts has low thermal conductivity since the spins do not talk to each other in the “gas” states, here in the spin-1 compounds heat can be transferred through the magnetic excitations between the coupled spins. This renders the spin-1 magnet DTN a very promising quantum magnetic refrigerant with both high cooling capacities and excellent performance.

The compounds DTN and TMNIN are very classic spin-1 chain materials and their single-crystal samples have been synthesized for quite some time. For example, high-quality

single-crystal of DTN has been used in the studies of Bose-Einstein condensation in quantum magnets [34, 35] and thermal transport measurements [23, 37]. Therefore, above we only consider the iMCE in single-crystal DTN samples, and the fields are applied along the the single-ion c axis. In case that only powder samples are available, or when the field tilts an angle with respect to the single-crystal c axis, we need to consider the iMCE properties of DTN under a tilted field. We have also performed the calculations and found the field-induced QCP as well as enhanced iMCE are still present for a range of tilting angles (see Appendix B).

Lastly, normal and inverse MCE properties for magnets with high Curie temperatures have been intensively discussed for room- or near room-temperature refrigeration [50–54], which helps enhance the cooling capacity and design a compact continuous refrigeration machinery [55]. Similarly, the efficient iMCE refrigerant, e.g., spin-1 DTN here, is important for designing a low- T continuous cooling cycle where temperature can be decreased in both the magnetization and demagnetization processes. Our work fills this gap by finding DTN a very promising iMCE compound that provides a high-performance refrigerants in the “arsenal” of spin-chain quantum materials.

ACKNOWLEDGMENTS

This work was supported by the National Natural Science Foundation of China (Grant Nos. 11704113, 11834014, 11974036, 12074024), Natural Science Foundation of Hunan Province, China (Grant No. 2018JJ3111) and the Scientific Research Fund of Hunan Provincial Education Department of China (Grant No. 19B159).

Appendix A: Linearized tensor renormalization group method

Thermodynamics of the spin-chain models and materials can be calculated via the thermal-state tensor renormalization group (TRG) methods. In this work, we employ the linearized TRG (LTRG) [21, 22] proposed by some of the authors to perform the finite- T simulations. For the spin-1 chain model Eq. (1), the Hamiltonian can be divided into odd and even parts through the Trotter-Suzuki decomposition [56], and the thermal density matrix can be expressed as

$$\hat{\rho}_\beta = e^{-\beta H} = (e^{-\tau H})^n \simeq (e^{-\tau H_{\text{odd}}} e^{-\tau H_{\text{even}}})^n, \quad (\text{A1})$$

where n is a sufficiently large integer and the (small) imaginary time slice is $\tau = \beta/n$. In practice, τ is chosen as 0.05 and we iteratively project the imaginary evolution gates $e^{-\tau H}$ of a single Trotter step to the matrix-product density operator, so as to cool down the temperature. In the bilayer algorithm, the density matrix at an inverse temperature β is obtained by

$$\hat{\rho}_\beta = \hat{\rho}_{\beta/2}^\dagger \cdot \hat{\rho}_{\beta/2}, \quad (\text{A2})$$

which saves the cost of calculations (by half) and improve considerably the accuracy by assuring positivity of the density matrix [22].

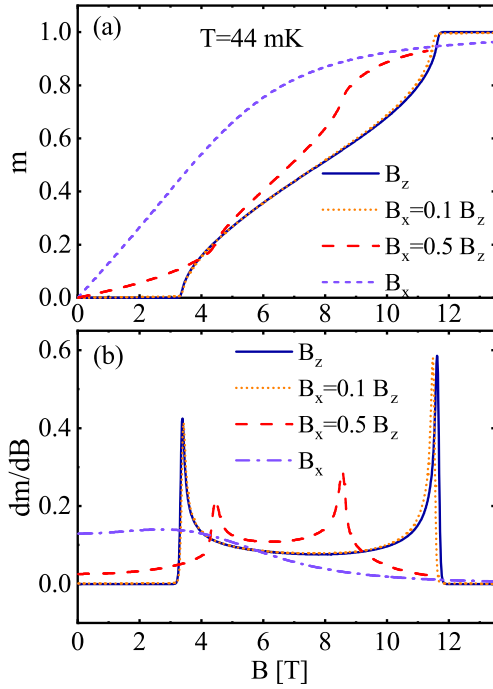


Fig. 8. (a) Low-temperature magnetization curves under magnetic fields along various directions including the c axis (longitudinal field B_z), tilted directions $B_x/B_z = 0.1, 0.5$, and the transverse field (B_x). (b) shows the derivative dm/dB of the three cases.

Appendix B: Quantum phase transition and magnetocaloric effects under tilted fields

When only powder samples are available or a small misalignment of the field direction occurs for single-crystal sample, the iMCE properties of DTN need to be reconsidered as the fields can be applied along directions other than the single-ion c axis. In Fig. 8, we show the low- T magnetization process along the tilted directions as described by the Hamiltonian

$$\mathcal{H} = \sum_i J \vec{S}_i \cdot \vec{S}_{i+1} + D(S_i^z)^2 + g\mu_B(B_x S_i^x + B_z S_i^z),$$

with the total field strength $B = \sqrt{B_x^2 + B_z^2}$. In Fig. 8 we computed the cases $B_x = 0.1 B_z$ ($\theta = 5.71^\circ$) and $B_x = 0.5 B_z$ ($\theta = 26.6^\circ$), and find there still exists criticality-enhanced iMCE when tilting the longitudinal from the c axis with an angle θ . Correspondingly, in Fig. 9 we see clear iMCE effect near the field-induced QCPs, including the evident temperature decrease and clear dip in the Grüneisen parameter Γ_B .

On the other hand, when the field is applied perpendicular to the single-ion axis (i.e., B_x with $\theta = 90^\circ$), indeed we observe that the QCP is absent (Fig. 8) and thus no pronounced iMCE can be observed. Based these calculations, we find the quantum criticality enhanced iMCE exists for certain tilted fields, but not for too large tilting angles (e.g., a perpendicular B_x). Nevertheless, when the tilting angle is small

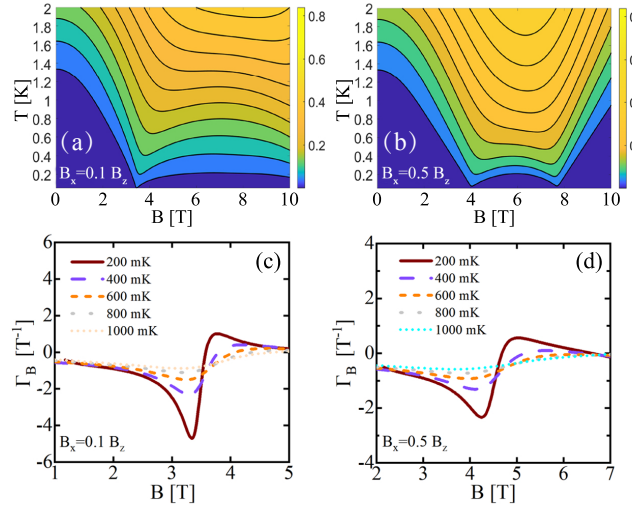


Fig. 9. (a, b) show the simulated isentropic contours and (c, d) are the Grüneisen parameters under tilted fields ($B_x/B_z = 0.1$ and 0.5). The lower critical fields are slightly modified in the two cases, and Γ_B dip characterizing iMCE becomes less pronounced for $B_x = 0.5 B_z$ as compared to that of $B_x = 0.1 B_z$.

(e.g., $\theta = 5.71^\circ$), we find the iMCE rather robust and barely changed as compared to that along the c axis.

[1] E. Warburg, Magnetische untersuchungen, *Ann. Phys.-Berlin* **249**, 141 (1881).
 [2] P. Weiss and A. Piccard, Le phénomène magnétocalorique, *J. Phys. (Paris)* **7**, 103 (1917).
 [3] O. Tegus, E. Brück, K. H. J. Buschow, and F. R. de Boer, Transition-metal-based magnetic refrigerants for room-temperature applications, *Nature* **415**, 150 (2002).
 [4] A. Smith, Who discovered the magnetocaloric effect?, *Eur. Phys. J. H* **38**, 507 (2013).
 [5] O. V. Lounasmaa, *Experimental principles and methods below 1K* (ACADEMIC, 1974).
 [6] C. Hagmann and P. L. Richards, Adiabatic demagnetization refrigerators for small laboratory experiments and space astron-

omy, *Cryogenics* **35**, 303 (1995).
 [7] P. J. Shirron, Cooling Capabilities of Adiabatic Demagnetization Refrigerators, *J. Low Temp. Phys.* **148**, 915 (2007).
 [8] A. E. Jahromi, P. J. Shirron, and M. J. DiPirro, *Sub-Kelvin Cooling Systems for Quantum Computers*, Tech. Rep. (NASA Goddard Space Flight Center Greenbelt, MD, United States, 2019).
 [9] M. E. Zhitomirsky, Enhanced magnetocaloric effect in frustrated magnets, *Phys. Rev. B* **67**, 104421 (2003).
 [10] M. E. Zhitomirsky and A. Honecker, Magnetocaloric effect in one-dimensional antiferromagnets, *J. Stat. Mech.: Theor. Exp.* **2004**, 07012 (2004).
 [11] L. J. Zhu, M. Garst, A. Rosch, and Q. M. Si, Universally Diverging Grüneisen Parameter and the Magnetocaloric Effect

- Close to Quantum Critical Points, *Phys. Rev. Lett.* **91**, 066404 (2003).
- [12] M. Garst and A. Rosch, Sign change of the Grüneisen parameter and magnetocaloric effect near quantum critical points, *Phys. Rev. B* **72**, 205129 (2005).
- [13] A. Honecker and S. Wessel, Magnetocaloric effect in quantum spin- s chains, *Condens. Matter Phys.* **12**, 399 (2009).
- [14] J. W. Sharples, D. Collison, E. J. L. McInnes, J. Schnack, E. Palacios, and M. Evangelisti, Quantum signatures of a molecular nanomagnet in direct magnetocaloric measurements, *Nat. Commun.* **5**, 5321 (2014).
- [15] M. Orendáč, R. Tarasenko, V. Tkáč, A. Orendáčová, and V. Sechovský, Specific heat study of the magnetocaloric effect in the Haldane-gap $S=1$ spin-chain material $[\text{Ni}(\text{C}_2\text{H}_8\text{N}_2)_2\text{NO}_2](\text{BF}_4)$, *Phys. Rev. B* **96**, 094425 (2017).
- [16] B. Wolf, Y. Tsui, D. Jaiswal-Nagar, U. Tutsch, A. Honecker, K. Remović-Langer, G. Hofmann, A. Prokofiev, W. Assmus, G. Donath, and M. Lang, Magnetocaloric effect and magnetic cooling near a field-induced quantum-critical point, *Proc. Natl. Acad. Sci.* **108**, 6862 (2011).
- [17] M. Lang, B. Wolf, A. Honecker, L. Balents, U. Tutsch, P. T. Cong, G. Hofmann, N. Krüger, F. Ritter, W. Assmus, and A. Prokofiev, Field-induced quantum criticality - application to magnetic cooling, *Phys. Status Solidi B* **250**, 457 (2013).
- [18] U. Schollwöck, J. Richter, D. J. J. Farnell, and R. F. Bishop, *Quantum Magnetism*, Vol. 645 (2004).
- [19] S. Sachdev, *Quantum Phase Transitions*, Vol. 12 (2011).
- [20] P. Gegenwart, Grüneisen parameter studies on heavy fermion quantum criticality, *Rep. Prog. Phys.* **79**, 114502 (2016).
- [21] W. Li, S. J. Ran, S. S. Gong, Y. Zhao, B. Xi, F. Ye, and G. Su, Linearized tensor renormalization group algorithm for the calculation of thermodynamic properties of quantum lattice models, *Phys. Rev. Lett.* **106**, 127202 (2011).
- [22] Y. L. Dong, L. Chen, Y. J. Liu, and W. Li, Bilayer linearized tensor renormalization group approach for thermal tensor networks, *Phys. Rev. B* **95**, 144428 (2017).
- [23] X. F. Sun, W. Tao, X. M. Wang, and C. Fan, Low-Temperature Heat Transport in the Low-Dimensional Quantum Magnet $\text{NiCl}_2\text{-4SC}(\text{NH}_2)_2$, *Phys. Rev. Lett.* **102**, 167202 (2009).
- [24] J. C. Bonner, Generalized Heisenberg quantum spin chains (invited), *J. Appl. Phys.* **61**, 3941 (1987).
- [25] O. Golinelli, T. Jolicœur, and R. Lacaze, Dispersion of magnetic excitations in a spin-1 chain with easy-plane anisotropy, *Phys. Rev. B* **46**, 10854 (1992).
- [26] F. D. M. Haldane, Nonlinear field theory of large-spin Heisenberg antiferromagnets: Semiclassically quantized solitons of the one-dimensional easy-axis Néel state, *Phys. Rev. Lett.* **50**, 1153 (1983).
- [27] M. P. Nightingale and H. W. J. Blote, Gap of the linear spin-1 Heisenberg antiferromagnet: A Monte Carlo calculation, *Phys. Rev. B* **33**, 659 (1986).
- [28] S. R. White and D. A. Huse, Numerical renormalization-group study of low-lying eigenstates of the antiferromagnetic $S=1$ Heisenberg chain, *Phys. Rev. B* **48**, 3844 (1993).
- [29] T. Sakai and M. Takahashi, Effect of the Haldane gap on quasi-one-dimensional systems, *Phys. Rev. B* **42**, 4537 (1990).
- [30] V. Gadet, M. Verdaguer, V. Briois, A. Gleizes, J. P. Renard, P. Beauvillain, C. Chappert, T. Goto, K. Le Dang, and P. Veillet, Structural and magnetic properties of $(\text{CH}_3)_4\text{NNi}(\text{NO}_2)_3$: A Haldane-gap system, *Phys. Rev. B* **44**, 705 (1991).
- [31] T. Takeuchi, H. Hori, M. Date, T. Yosida, K. Katsumata, J. Renard, V. Gadet, and M. Verdaguer, High field magnetization of Haldane materials TMNIN and NINAZ, *J. Magn. Magn. Mater.* **104**, 813 (1992).
- [32] M. Ito, M. Mito, H. Deguchi, and K. Takeda, The Numerical Comparison of Magnetic Susceptibility and Heat Capacity of TMNIN with the Result of a Quantum Monte Carlo Method for the Haldane System, *J. Phys. Soc. Jpn.* **63**, 1123 (1994).
- [33] T. Goto, T. Ishikawa, Y. Shimaoka, and Y. Fujii, Quantum spin dynamics studied by the nuclear magnetic relaxation of protons in the Haldane-gap system $(\text{CH}_3)_4\text{NNi}(\text{NO}_2)_3$, *Phys. Rev. B* **73**, 214406 (2006).
- [34] V. S. Zapf, D. Zocco, B. R. Hansen, M. Jaime, N. Harrison, C. D. Batista, M. Kenzelmann, C. Niedermayer, A. Lacerda, and A. Paduan-Filho, Bose-Einstein condensation of $S=1$ nickel spin degrees of freedom in $\text{NiCl}_2\text{-4SC}(\text{NH}_2)_2$, *Phys. Rev. Lett.* **96**, 077204 (2006).
- [35] A. Paduan-Filho, K. A. Al-Hassanieh, P. Sengupta, and M. Jaime, Critical properties at the field-induced bose-einstein condensation in $\text{NiCl}_2\text{-4SC}(\text{NH}_2)_2$, *Phys. Rev. Lett.* **102**, 077204 (2009).
- [36] O. Chiatti, S. Zherlitsyn, A. Sytcheva, J. Wosnitza, A. A. Zvyagin, V. S. Zapf, M. Jaime, and A. Paduan-Filho, Ultrasonic investigation of $\text{NiCl}_2\text{-4SC}(\text{NH}_2)_2$, *Journal of Physics: Conference Series* **150**, 042016 (2009).
- [37] Y. Kohama, A. V. Sologubenko, N. R. Dilley, V. S. Zapf, M. Jaime, J. A. Mydosh, A. Paduan-Filho, K. A. Al-Hassanieh, P. Sengupta, S. Gangadharaiah, A. L. Chernyshev, and C. D. Batista, Thermal transport and strong mass renormalization in $\text{NiCl}_2\text{-4SC}(\text{NH}_2)_2$, *Phys. Rev. Lett.* **106**, 037203 (2011).
- [38] C. Psaroudaki, S. A. Zvyagin, J. Krzystek, A. Paduan-Filho, X. Zotos, and N. Papanicolaou, Magnetic excitations in the spin-1 anisotropic antiferromagnet $\text{NiCl}_2\text{-4SC}(\text{NH}_2)_2$, *Phys. Rev. B* **85**, 014412 (2012).
- [39] E. Čížmár, M. Ozerov, O. Ignatchik, T. P. Papageorgiou, J. Wosnitza, S. A. Zvyagin, J. Krzystek, Z. Zhou, C. P. Landee, B. R. Landry, M. M. Turnbull, and J. L. Wikaira, Magnetic properties of the Haldane-gap material $[\text{Ni}(\text{C}_2\text{H}_8\text{N}_2)_2\text{NO}_2](\text{BF}_4)$, *New J. Phys.* **10**, 033008 (2008).
- [40] J. P. Renard, M. Verdaguer, L. P. Regnault, W. A. C. Erkelens, J. Rossat-Mignod, J. Ribas, W. G. Stirling, and C. Vettier, Quantum energy gap in two quasi-one dimensional $S=1$ Heisenberg antiferromagnet, *J. App. Phys.* **63**, 3538 (1988).
- [41] T. Kobayashi, Y. Tabuchi, K. Amaya, Y. Ajiro, T. Yosida, and M. Date, Heat capacities of haldane-gap antiferromagnet NENP in magnetic field, *J. Phys. Soc. Jpn.* **61**, 1772 (1992).
- [42] T. Takeuchi, M. Ono, H. Hori, T. Yosida, A. Yamagishi, and M. Date, Magnetization measurement of NENP and NINO in high magnetic field, *J. Phys. Soc. Jpn.* **61**, 3255 (1992).
- [43] W. Tao, L. M. Chen, X. M. Wang, C. Fan, W. P. Ke, X. G. Liu, Z. Y. Zhao, Q. J. Li, and X. F. Sun, Crystal growth and characterization of Haldane chain compound $\text{Ni}(\text{C}_3\text{H}_{10}\text{N}_2)_2\text{NO}_2\text{ClO}_4$, *J. Cryst. Growth* **327**, 215 (2011).
- [44] A. Zheludev, S. E. Nagler, S. M. Shapiro, L. K. Chou, D. R. Talham, and M. W. Meisel, Spin dynamics in the linear-chain $s=1$ antiferromagnet $\text{Ni}(\text{C}_3\text{H}_{10}\text{N}_2)_2\text{N}_3(\text{ClO}_4)$, *Phys. Rev. B* **53**, 15004 (1996).
- [45] K. Kordonis, A. V. Sologubenko, T. Lorenz, S.-W. Cheong, and A. Freimuth, Spin thermal conductivity of the haldane chain compound Y_2BaNiO_5 , *Phys. Rev. Lett.* **97**, 115901 (2006).
- [46] J. J. Li, Z. W. Ouyang, Y. C. Sun, X. Y. Yue, Z. C. Xia, and G. H. Rao, Magnetic Enhancement and Suppression of Haldane Gap in Nanocrystals of Spin-Chain Y_2BaNiO_5 , *J. Low Temp. Phys.* **188**, 11 (2017).
- [47] Z.-C. Gu and X.-G. Wen, Tensor-entanglement-filtering renormalization approach and symmetry-protected topological order, *Phys. Rev. B* **80**, 155131 (2009).
- [48] A. V. Prokofiev, W. Assmus, K. Remović-Langer,

- V. Pashchenko, Y. Tsui, B. Wolf, and M. Lang, Crystal growth and magnetic properties of the copper coordination polymer $[\text{Cu}(\mu\text{-C}_2\text{O}_4)(4\text{-aminopyridine})_2(\text{H}_2\text{O})]_n$, *Cryst. Res. Technol.* **42**, 394 (2007).
- [49] T. Takeuchi, H. Hori, T. Yosida, A. Yamagishi, K. Katsumata, J. P. Renard, V. Gadet, M. Verdaguer, and M. Date, Magnetization process of Haldane materials TMNIN and NINAZ, *Journal of the Physical Society of Japan* **61**, 3262 (1992).
- [50] T. Krenke, E. Duman, M. Acet, E. F. Wassermann, X. Moya, L. Manosa, and A. Planes, Inverse magnetocaloric effect in ferromagnetic Ni-Mn-Sn alloys, *Nat. Mater.* **4**, 450 (2005).
- [51] X. Moya, L. Mañosa, A. Planes, S. Aksoy, M. Acet, E. F. Wassermann, and T. Krenke, Cooling and heating by adiabatic magnetization in the $\text{Ni}_{50}\text{Mn}_{34}\text{In}_{16}$ magnetic shape-memory alloy, *Phys. Rev. B* **75**, 184412 (2007).
- [52] V. B. Naik and R. Mahendiran, Normal and inverse magnetocaloric effects in ferromagnetic $\text{Sm}_{0.6-x}\text{La}_x\text{Sr}_{0.4}\text{MnO}_3$, *J. Appl. Phys.* **110**, 053915 (2011).
- [53] D. V. Maheswar Repaka, M. Aparnadevi, P. Kumar, T. S. Tripathi, and R. Mahendiran, Normal and inverse magnetocaloric effects in ferromagnetic $\text{Pr}_{0.58}\text{Sr}_{0.42}\text{MnO}_3$, *J. Appl. Phys.* **113**, 17A906 (2013).
- [54] R. Das, P. Yanda, A. Sundaresan, and D. D. Sarma, Ground-state ferrimagnetism and magneto-caloric effects in $\text{Nd}_2\text{NiMnO}_6$, *Mater. Res. Express* **6**, 116122 (2019).
- [55] X. Zhang, B. Zhang, S. Yu, Z. Liu, W. Xu, G. Liu, J. Chen, Z. Cao, and G. Wu, Combined giant inverse and normal magnetocaloric effect for room-temperature magnetic cooling, *Phys. Rev. B* **76**, 132403 (2007).
- [56] M. Suzuki, Relationship between d-Dimensional Quantal Spin Systems and (d+1)-Dimensional Ising Systems —Equivalence, Critical Exponents and Systematic Approximants of the Partition Function and Spin Correlations—, *Prog. Theor. Phys.* **56**, 1454 (1976).